

Cite this: *Photochem. Photobiol. Sci.*, 2014, **13**, 563

## Photochemistry of 6-amino-2-azido, 2-amino-6-azido and 2,6-diazido analogues of purine ribonucleosides in aqueous solutions†

Krzysztof Komodziński,<sup>a</sup> Jolanta Lepczyńska,<sup>a</sup> Zofia Gdaniec,<sup>b</sup> Libero Bartolotti,<sup>c</sup> Bernard Delley,<sup>d</sup> Stefan Franzen<sup>e</sup> and Bohdan Skalski\*<sup>a</sup>

The photochemistry of 6-amino-2-azidopurine, 2-amino-6-azidopurine and 2,6-diazidopurine ribonucleosides has been investigated in aqueous solutions under aerobic and anaerobic conditions. Near UV irradiation of 6-amino-2-azido-9-(2',3',5'-tri-*O*-acetyl-β-*D*-ribofuranosyl)purine and 2-amino-6-azido-9-(2',3',5'-tri-*O*-acetyl-β-*D*-ribofuranosyl)purine in the presence of oxygen leads to efficient formation of 6-amino-2-nitro-9-(2',3',5'-tri-*O*-acetyl-β-*D*-ribofuranosyl)purine and 2-amino-6-nitro-9-(2',3',5'-tri-*O*-acetyl-β-*D*-ribofuranosyl)purine. Under anaerobic conditions, both azidopurine ribonucleosides preferentially undergo photoreduction to 2,6-diamino-9-(2',3',5'-tri-*O*-acetyl-β-*D*-ribofuranosyl)purine. The structures of the photoproducts formed were confirmed by UV, NMR and HR ESI-TOF MS spectral data. The photoproducts observed in this study for the aminoazidopurines are distinctly different from those observed previously for 6-azidopurine. When no amino group is present, the photochemistry of 6-azidopurine leads to the formation of a 1,3,5-triazepinone nucleoside. The energetics of the 6-nitreno moiety along both oxidation and ring expansion pathways was calculated using the nudged elastic band (NEB) method based on density functional theory (DFT) using DMol3. The role of the 2-amino group in regulating the competition between these pathways was elucidated in order to explain how the striking difference in reactivity under irradiation arises from the greater spin density on the 6-nitreno-9-methyl-9*H*-purin-2-amine, which essentially eliminates the barrier to oxidation observed in 6-nitreno-9-methyl-9*H*-purine. Finally, the importance of tetrazolyl intermediates for the photochemical activation of azide bond cleavage to release N<sub>2</sub> and form the 6-nitreno group was also corroborated using the DFT methods.

Received 5th November 2013,  
Accepted 27th December 2013

DOI: 10.1039/c3pp50385b

www.rsc.org/ppps

## Introduction

Nucleosides bearing azido group(s) attached directly to a heterocyclic ring belong to a wide range of aryl azides that are commonly used as photoaffinity labeling probes for the study of the structure and function of biological macromolecules.<sup>1</sup> Several features of these azidonucleosides, such as their high photochemical reactivity and ability to form covalent bonds

with a variety of biomolecular constituents in their immediate environment upon near UV activation, their straightforward synthesis and the availability of both enzymatic and chemical procedures for their incorporation into DNA and RNA polynucleotides, the close structural similarity to their parent nucleobases and their good chemical stability in the absence of light, make these compounds unique in their use as photocrosslinking reagents.<sup>2</sup>

Understanding the photochemical behavior of azidonucleosides alone, by determining their structures and mechanisms of photoproduct formation, is important in relation to understanding the mechanisms of the reactions and the prediction of structures of the adducts formed under crosslinking conditions. Surprisingly, in spite of the extensive application of azidonucleosides as photoaffinity probes, their photochemistry remains rather poorly understood.<sup>2</sup> Several photochemical studies of various azido substituted pyrimidine compounds have been carried out.<sup>3</sup> However, among azidopurine ribonucleosides, only the photochemical reactions of 2-azidoadenosine<sup>4</sup> in alcohols and 8-azido- and 6-azidopurine ribonucleosides in

<sup>a</sup>Faculty of Chemistry, Adam Mickiewicz University, Umultowska 89b, 61-614 Poznań, Poland. E-mail: bskalski@amu.edu.pl; Fax: +48-61-829-6761; Tel: +48-61-829-1585

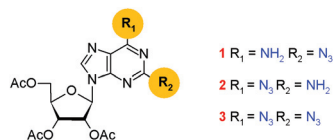
<sup>b</sup>Institute of Bioorganic Chemistry, Polish Academy of Science, Z. Noskowskiego 12/14, 61-704 Poznań, Poland

<sup>c</sup>Department of Chemistry, East Carolina University, Greenville, NC 27858, USA

<sup>d</sup>Paul-Scherer Institute, CH-5232 Villigen, Switzerland

<sup>e</sup>Department of Chemistry, North Carolina State University, Raleigh, NC 27695, USA

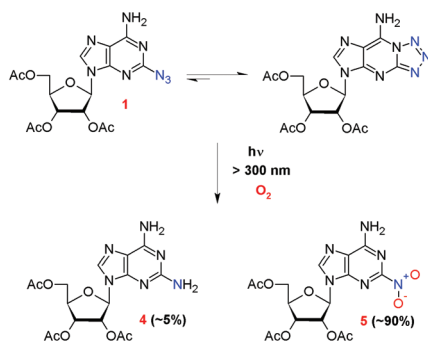
†Electronic supplementary information (ESI) available: The HR ESI-TOF MS, <sup>1</sup>H NMR, <sup>13</sup>C NMR and <sup>1</sup>H-<sup>13</sup>C HMBC spectral data of photoproducts 5 and 7. The HPLC analyses of photoirradiated solutions of compound 3. See DOI: 10.1039/c3pp50385b



**Scheme 1** The structures of compounds 1–3.

aqueous solutions have been investigated.<sup>5,6</sup> It has been shown that the photochemistry of these aryl azides is quite complex and highly dependent on the position of the azide group in a heterocyclic ring, the presence of various substituents, the solvents used and the tendency to exist in the solvent and pH dependent azide-tetrazole tautomeric equilibria.<sup>3</sup> In the case of 2-azidoadenosine, the formation of 8-substituted products in addition to the reduction of the nitrene at the 2-position was observed.<sup>4</sup> Efficient reduction of the nitrene occurs also in the case of 8-azidoadenosine, which undergoes transformation into 8-aminoadenosine upon UV irradiation in aqueous solutions,<sup>5</sup> whereas this is only a minor process in the case of 6-azidopurine ribonucleoside.<sup>6</sup> As we have shown, the photochemical behavior of the latter resembles closely that of 4- and 6-azidouracils,<sup>3e,h</sup> namely it undergoes efficient photochemical purine ring expansion leading to the novel imidazole-fused 1,3,5-triazepinone nucleoside.<sup>6</sup> Furthermore, our recent study showed that selective excitation of 6-azidopurine incorporated into single stranded DNA oligonucleotide leads to the analogous purine ring expanded product.<sup>7</sup> These large differences in reactivity have not been explained.

In this contribution, we report on a study of the photochemistry of 2-azido-6-aminopurine-, 6-azido-2-aminopurine- and 2,6-diazidopurine ribonucleosides 1–3 (Scheme 1) in aqueous solution under aerobic and anaerobic conditions. As will be shown, none of these azidopurines undergoes ring expansion. Instead, depending on the conditions of irradiation, photoreactions of the two amino-substituted derivatives are dominated by photooxidation and/or photo-reduction of the nitrene leading to respective nitro and/or amino derivatives (Scheme 2). We have rationalized the differences in photochemical reactivity of the 6-azidopurine and 6-azido-2-aminopurine systems, based on quantum chemical



**Scheme 2** Azide-tetrazole tautomeric equilibrium of 1 in aqueous solution<sup>10</sup> and structures of photoproducts of its irradiation under aerobic conditions.

calculations. Application of computational methods to these problems has synergy with experimental approaches leading to a deeper understanding of the mechanistic aspects, which govern the reactivity of azido-nucleosides.

## Results and discussion

### Photochemistry of azidopurine nucleosides 1–3

Aqueous solutions of compounds 1–3 were irradiated at  $\lambda > 300 \text{ nm}$  under aerobic and anaerobic conditions at room temperature and the progress of the photoreactions was monitored by both UV-Vis spectroscopy and HPLC. As shown in Fig. 1, irradiation of an aqueous solution of 1, under both aerobic and anaerobic conditions, results in almost complete conversion after 12 min, indicating that the presence of oxygen has virtually no effect on the relative quantum yield of disappearance of 1. The HPLC analysis of the solution of 1 irradiated under aerobic conditions showed the presence of two peaks, 4 and 5, corresponding to the minor and the major photoproduct, respectively, whereas in the case of irradiation of 1 under anaerobic conditions, the formation of 4 as the only major photoproduct was observed. The photoproducts 4 and 5 were isolated and purified by preparative reversed-phase HPLC. The

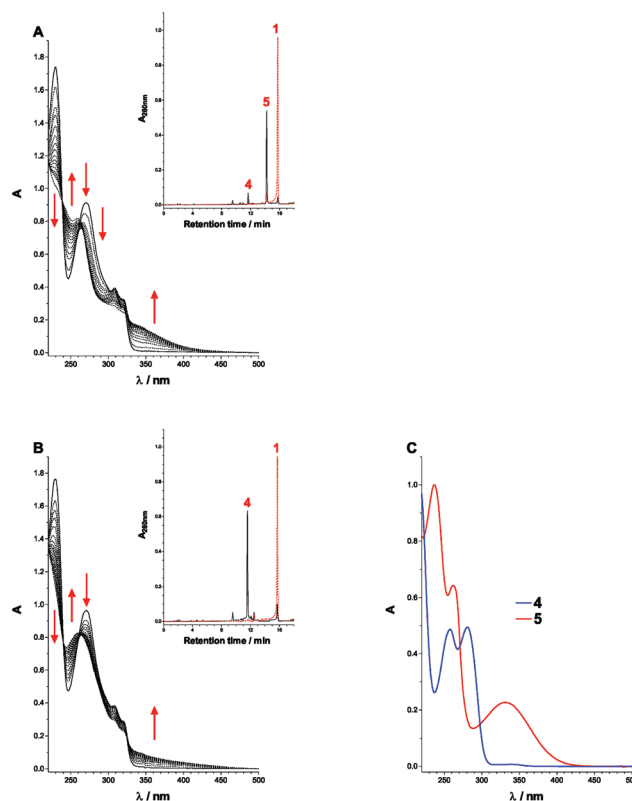


**Fig. 1** Changes in the absorption spectrum of an aqueous solution of 1 measured with 1 min increments during irradiation at  $\lambda > 300 \text{ nm}$  under aerobic (A) and anaerobic (B) conditions together with HPLC analyses of the solutions (inset) before irradiation (dotted red lines) and after 12 min irradiation (solid black lines). (C) The normalized absorption spectra of the photoproducts 4 and 5.

photoproduct **4** was identified as 2,6-diamino-9-(2',3',5'-tri-*O*-acetyl- $\beta$ -*D*-ribofuranosyl)purine based on HR ESI-TOF MS and NMR spectral data and comparison of its UV spectrum with the published one.<sup>8</sup>

The molecular formula of **5** (C<sub>16</sub>H<sub>18</sub>N<sub>6</sub>O<sub>9</sub>), inferred from the high-resolution ESI-TOF MS spectrum, indicated that the formation of this photoproduct involves the loss of a N<sub>2</sub> molecule and addition of an O<sub>2</sub> molecule. As shown in Fig. 1C the UV spectrum of photoproduct **5** displays three maxima at  $\lambda$  236 nm, 262 nm, and 332 nm characteristic of the 2-nitroadenosine chromophore.<sup>9</sup> The identity of **5** with the latter was further supported by the <sup>1</sup>H and <sup>13</sup>C NMR spectra.

The <sup>1</sup>H NMR spectrum of **5** showed the signal patterns typical of the intact *O*-acetylated ribose and two signals at 8.19 and 6.18 ppm corresponding to C8-H and C6-NH<sub>2</sub> of the purine aglycone, respectively. The <sup>13</sup>C NMR spectrum displayed five carbon signals in its aromatic region, one methine carbon (C8) at 141.8 ppm and four quaternary carbons at 155.9, 155.4, 149.8 and 122.1 ppm. The <sup>1</sup>H-<sup>13</sup>C HSQC spectrum showed a correlation of H8 (8.19 ppm) with C8 (141.8 ppm) and the <sup>1</sup>H-<sup>13</sup>C HMBC spectrum showed correlations of H8 (8.19 ppm) with C4 (149.8 ppm) and C5 (122.1 ppm); H1' (6.26 ppm) with C4 (149.8 ppm) and C8 (141.8 ppm).

The photochemical behavior of the 2-amino-6-azidopurine nucleoside **2** is similar to that of its 6-amino-2-azido isomer **1**. As shown in Fig. 2, irradiation under both aerobic and anaerobic conditions leads to complete conversion of **2** after 20 min with the relative quantum yield of disappearance similar to that of **1**. As in the case of **1**, the presence of oxygen has an effect only on the type and distribution of the photoproducts formed.

In the case of anaerobic irradiation of **2** the formation of 2,6-diaminopurine nucleoside **4** as the only major product (>90%) is observed, whereas under aerobic conditions, photo-oxidation of the azido group leading to the 6-nitro-2-aminopurine nucleoside **7** (50%) dominates, and photoreduction to **4** occurs to a much lesser extent (40%) (Scheme 3).

The proposed structure of **7**, which is a structural isomer of **5**, is in full agreement with the molecular formula C<sub>16</sub>H<sub>18</sub>N<sub>6</sub>O<sub>9</sub> determined by high-resolution ESI-TOF MS. As in the case of **5**, the <sup>1</sup>H NMR and <sup>13</sup>C NMR spectra of **7** show the peaks characteristic of the sugar and purine units of the molecule. In the <sup>1</sup>H NMR spectrum, two signals corresponding to C8-H and N-H<sub>2</sub> protons appear at 8.17 ppm and 5.62 ppm, respectively, in addition to resonances due to the ribose unit. In the aromatic region of the <sup>13</sup>C NMR spectrum of **7**, five signals appear, one from the methine carbon C8 (144.8 ppm) and four from quaternary carbons at 158.6, 158.3, 152.4 and 119.5 ppm. Heteromolecular carbon-proton one bond correlation was detected between C8 (144.8 ppm) and H8 (8.17 ppm). The <sup>1</sup>H-<sup>13</sup>C HMBC spectrum showed correlations between H8 (8.17 ppm) and both C5 (119.5 ppm) and C4 (152.4 ppm); anomeric H1' (6.11 ppm) with C4 (152.4 ppm) and C8 (144.8 ppm). Similarly, like in the case of **5**, the UV absorption spectrum of **7** displays the presence of an intense absorption

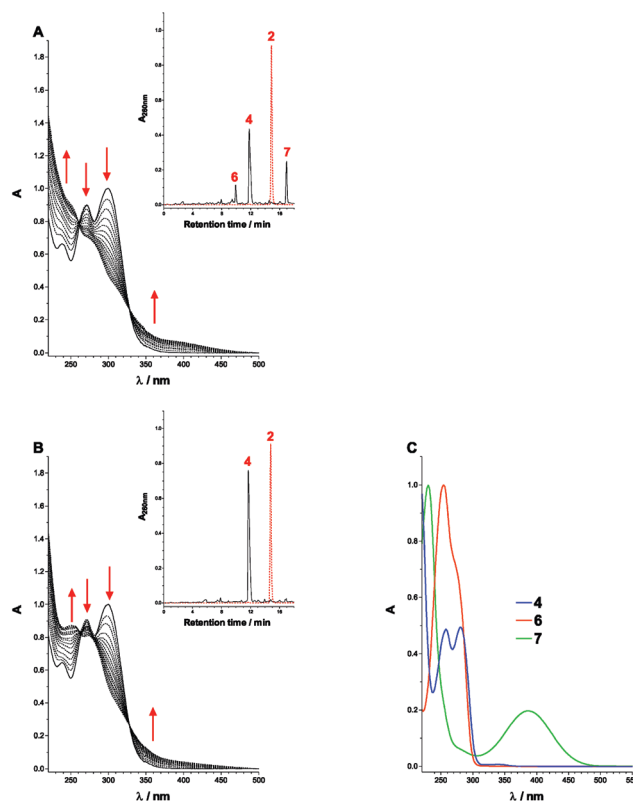
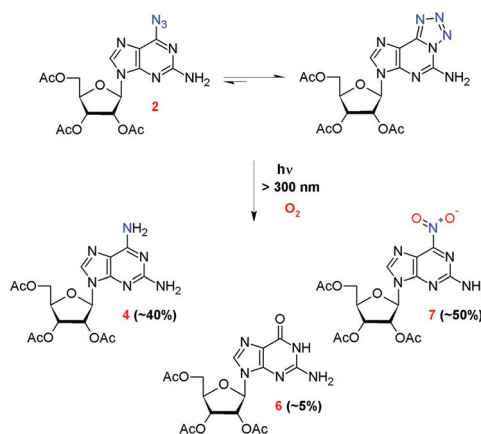


Fig. 2 Changes in the absorption spectrum of an aqueous solution of **2**, measured with 1 min increments, during irradiation at  $\lambda > 300$  nm under aerobic (A) and anaerobic (B) conditions together with HPLC analyses of the solutions (inset) before (dotted red lines) and after 20 min irradiation (solid black lines). (C) The normalized absorption spectra of photoproducts **4**, **6** and **7**.



Scheme 3 Azide-tetrazole tautomeric equilibrium of **2**<sup>11</sup> and structures of the photoproducts of its irradiation under aerobic conditions.

band at 230 nm ( $\epsilon = 14\,900\text{ M}^{-1}\text{ cm}^{-1}$ ) and a low intensity, broad absorption band centered at 386 nm ( $\epsilon = 2900\text{ M}^{-1}\text{ cm}^{-1}$ ) (Fig. 2C). To the best of our knowledge, the 2-amino-6-nitropurine chromophore has not been described previously in the literature.<sup>12</sup>

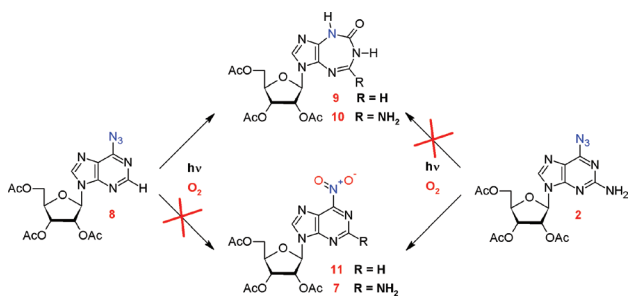
The minor photoproduct **6** of the aerobic irradiation of **2** (Fig. 2a) was identified as 2',3',5'-tri-*O*-acetylguanosine by comparison with authentic samples (UV spectrum and HPLC). Upon prolonged irradiation of the reaction mixture, an increase in the amount of **6** formed with a concomitant, gradual disappearance of **7** was observed indicating that the latter undergoes further phototransformation into **6**. This was further supported by direct irradiation of an isolated, pure sample of **7** under identical conditions (Fig. S9, ESI†).

In contrast to monoazide substituted purine nucleosides **1** and **2**, irradiation of the 2,6-diazidopurine derivative **3** leads to its very rapid disappearance with the formation of a complex mixture of more than 20 photoproducts (Fig. S10, ESI†) indicating its extensive degradation.

### Computational study of the photochemical pathways of 6-azidopurine and 2-amino-6-azidopurine

The above described photochemical pathways of amino-substituted azidopurines **1,2** differ significantly from that of the unsubstituted 6-azidopurine nucleoside (**8**) despite the fact that the primary photochemical event in each of these compounds involves elimination of N<sub>2</sub> leading to a highly reactive intermediate nitrene in the 6-position. It is indeed remarkable that 2-amino-6-nitrenopurine proceeds with high yield to form the 6-nitro group (**7**), while 6-nitrenopurine under analogous photoirradiation conditions reacts nearly quantitatively to form the 1,3,5-triazepin-2-one (**9**). These distinct paths are shown in Scheme 4.

In order to determine the origin of the difference in reactivity between 6-azidopurine (**8**) and 2-amino-6-azidopurine (**2**) nucleosides, the photochemical reactions of 9-methyl analogs of both nucleosides (**6AzP**, **2A6AzP**) were studied using density functional theory (DFT) as implemented in the DMol3 code<sup>13</sup> and nudged elastic band (NEB) calculation of the reaction path. There are two distinct phases for comparison. First, the formation of a tetrazole structure and the photolysis process that leads to formation of the 6-nitrenoadenine were studied for both the purine and 2-aminopurine. Then the analysis of the reaction path for oxidation was conducted by comparison with the alternative pathway for the formation of an imidazole-fused 1,3,5-triazepinone nucleoside.



Scheme 4

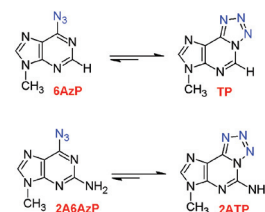
### Comparison of the formation of the 6-nitreno-9-methyl-9H-purine (**6NP**) and 6-nitreno-9-methyl-9H-purin-2-amine (**2A6NP**)

The photochemical reactions of 6-azido-9-methyl-9H-purine (**6AzP**) and 6-azido-9-methyl-9H-purin-2-amine (**2A6AzP**) shown in Scheme 5 compare the formation of a tetrazole structure in the two species, called **TP** and **2ATP**, respectively, and the photolysis process that leads to the formation of **6NP** in each case. First, the cyclizations of **6AzP** and **2A6AzP** to form a tetrazole ring in the cyclized form **TP** and **2ATP** were considered. Following irradiation, the stable tetrazole intermediates, **TP** and **2ATP**, lose N<sub>2</sub> to form reactive nitrene intermediates, 6-nitreno-9-methyl-9H-purine (**6NP**) and 6-nitreno-9-methyl-9H-purin-2-amine (**2A6NP**). Thus, this stage can be compared to the direct loss of the N<sub>2</sub> molecule from photoexcited **6AzP**.

The formation of nitrene has two alternative pathways. Direct cleavage of the N–N bond can lead to loss of N<sub>2</sub> and formation of 6-nitreno intermediate as shown in Fig. 3. The thermal energy barrier is 1.82 eV for this process.

The alternative pathway for the formation of **6NP** and **2A6NP** involves cyclization to form a tetrazole ring as shown in Scheme 4 and the NEB calculation for this pathway is shown in Fig. 4.

The loss of N<sub>2</sub> from **TP** and **2ATP** is shown in Fig. 5. This process parallels the loss of N<sub>2</sub> from **6AzP** shown in Fig. 3. The difference is seen in the first few frames of the NEB calculation. The small increase in the energy represents the



Scheme 5 Azide-tetrazole tautomeric equilibrium of **6AzP** and **2A6AzP** with **TP** and **2ATP**, respectively, in aqueous solution.

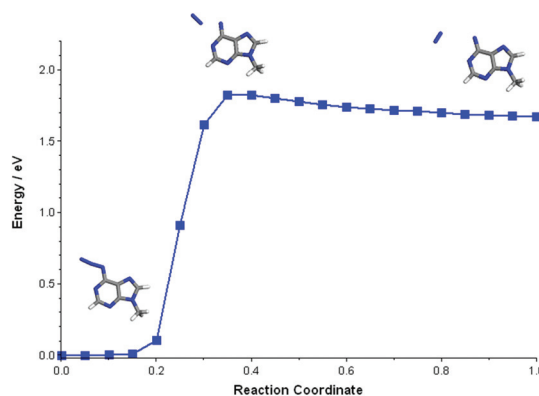
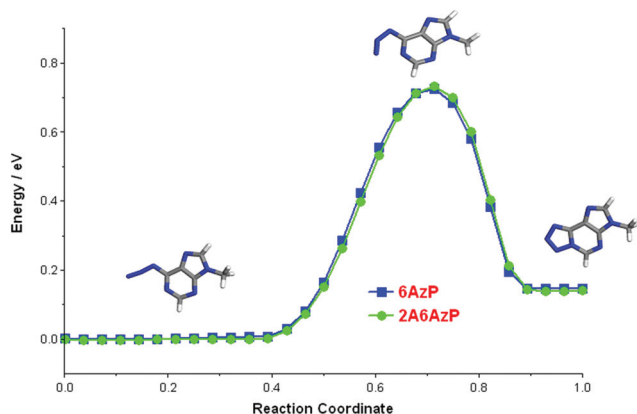
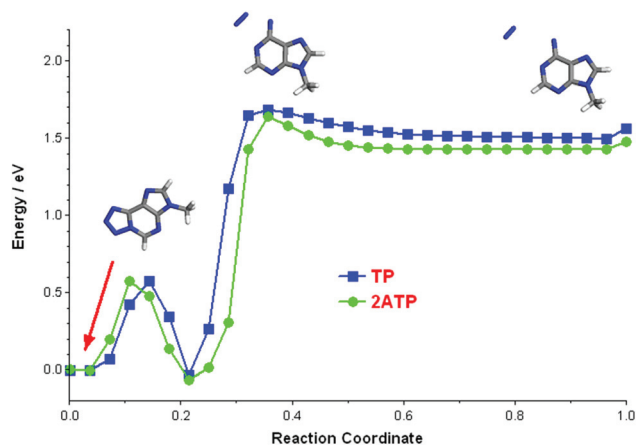


Fig. 3 Thermal dissociation of **6AzP** calculated using the NEB method. The structures corresponding to the reactant, transition state and product for the dissociation are shown immediately above the plot.



**Fig. 4** Comparison of the cyclization of the tetrazole ring in **6AzP** and **2A6AzP** calculated using the NEB method. The **6AzP** structures corresponding to the reactant, transition state and product for the cyclization are shown immediately above the plot. The analogous **2A6AzP** structures are omitted for clarity.



**Fig. 5** Comparison of the thermal dissociation of  $N_2$  from **TP** to form **6NP** and **2ATP** to form **2A6NP** calculated using the NEB method. The **TP** structures corresponding to the reactant, transition state and product for the dissociation are shown immediately above the plot. The analogous **2ATP** structures are omitted for clarity.

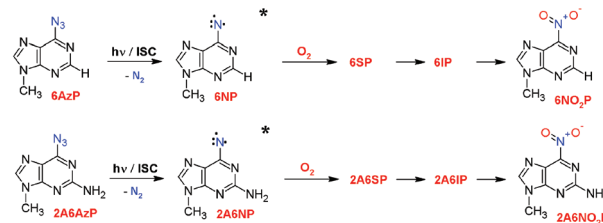
breaking of the first bond between the  $\gamma$  or terminal nitrogen,  $N_\gamma$ , of the azide and the  $N(5)$  nitrogen on the purine ring. Once this has taken place, the trajectory is quite similar to the photolysis of  $N_2$  from azide in **6AzP** except that the thermal barriers are 1.69 eV and 1.65 eV for **TP** and **2ATP**, respectively. In all cases the release of  $N_2$  is highly endothermic.

**6AzP**, **TP** and **2ATP** can each undergo photolysis of  $N_2$  to form the corresponding **6NP** intermediate. There are two reasons why **TP** may be favored over the **6AzP** form as the species that leads to photolysis. First, the **TP** isomer may be favored in solution. Second, the transition to the photolytic state may be favored in **TP**. The photoexcitations of **6AzP** and **TP** were compared using TD-DFT calculations in order to determine which of the transition moments is dominant. The nominal transitions are mainly 45→46 (*i.e.* HOMO→LUMO) for both **6AzP** and **TP**. As shown in Fig. S12 (ESI<sup>†</sup>), this

transition corresponds to a dissociative process with respect to loss of  $N_2$  for both molecules. The energies of the states involved in the photolysis of the 2-aminopurine tetrazole structure, **2ATP**, are shown in Fig. S13 (ESI<sup>†</sup>). It is evident that the features of **TP** are similar to those in **2ATP**. There are excited state curve crossings associated with the breaking of the first bond of the tetrazole ring (Fig. S13<sup>†</sup>). These facilitate passage of the system into the photolytic state. While this analysis is not rigorous it provides sufficient justification for our purposes, which is to differentiate the bent and cyclized (tetrazolyl) forms of the purines and provide a reasonable hypothesis for the photolytic state. We conclude that the photolytic state is most likely the tetrazolyl form (**TP** or **2ATP**). Secondly, our goal was to determine whether there is a substantial difference due to the presence of a 2-amino group on the purine photochemistry. Based on the similarity of the NEB trajectories and the excited state curve crossings observed at this level of theory, we conclude that the mechanisms of photolysis for both **TP** and **2ATP** are essentially the same. Clearly the excited state behavior will need to be studied using multiconfiguration methods to confirm the details of this conclusion and such studies will be forthcoming in our research. Since the formation of the tetrazole ring and photolysis appear quite similar in **TP** and **2ATP** these calculations support the hypothesis that the 6-nitreno group is prepared in a similar way irrespective of the presence of the 2-amino group. We conclude that the differences in reactivity of **6AzP** and **2A6AzP** are due to events that occur after photolysis, but there are no substantive differences in the photolytic step.

### Oxidation of nitrene intermediates

The oxidation path was chosen for analysis since  $O_2$  is the obvious oxidant and there is a clear starting point that involves approach by  $O_2$  to the 6-nitreno group. Thus, oxidation can be readily compared to the ring expansion pathway, while reduction is more difficult to model since the reductant is not known.<sup>14</sup> In order to understand the two competing reaction pathways, parallel calculations were set up as three distinct NEB calculations along the two competing reaction paths for each molecule. Path 1, which involves oxidation to the 6-nitro group, was separated into two stages since both **6NP** and **2A6NP** have a stable but high-energy 6-dioxaziridine intermediate, designated **6IP**, along the oxidation pathway (Scheme 6). Thus, it is reasonable to divide the NEB calculation for the oxidation part into two separate stages with the



**Scheme 6** Steps involved in path 1, which is the oxidation of the 6-nitreno group to the 6-nitro group.

intermediate as a stable point in the path. First is the association of O<sub>2</sub> to form the stable high-energy 6-dioxaziridine intermediate, which we call **6IP** from a transition state structure called **6SP**. Scheme 6 shows the parallel processes for the 2-aminopurine, which involves the transformation from **2A6SP** to **2A6IP**. The second step on path 1 is the formation of the 6-nitro group from the stable 6-dioxaziridine intermediate. Path 2 is the competing ring expansion, which occurs in a single step.

The high energy intermediate (**6IP**) shown in Fig. 6 has the appearance of a triangular molecule bent away from the plane of the purine ring. It is designated **6IP** to distinguish it from the product 6-nitropurine, **6NO<sub>2</sub>P**. The intermediate **6IP** can be geometry optimized and is clearly at a local minimum in the potential energy surface. It has defined vibrational frequencies with no aberrant eigenvalues meaning that all of its normal modes are well defined (see ESI†). However, the energy of **6IP** is higher than that of the **6NO<sub>2</sub>P** structure. Table 1 shows that the 2-amino group does not appear to have a large effect on the bond lengths or angles of either the intermediate **6IP** or the equilibrium 6-nitropurine structure (**6NO<sub>2</sub>P**).

The effective change along the reaction path from **6IP** to **6NO<sub>2</sub>P** is a rotation of one of the O atoms (labeled O(1)). The remaining atoms are in nearly the same positions in the two structures. The O atoms in the intermediate **6IP** form are tilted back away from the plane of the purine. The final equilibrium

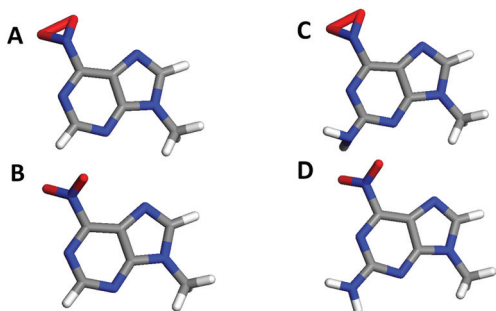


Fig. 6 Stick bond figure showing (A) the stable 6-dioxaziridino-9-methyl-9H-purine intermediate (**6IP**), (B) 6-nitro-9-methyl-9H-purine (**6NO<sub>2</sub>P**), (C) stable 6-dioxaziridino-9-methyl-9H-purin-2-amine intermediate (**2A6IP**), and (D) 6-nitro-9-methyl-9H-purin-2-amine (**2A6NO<sub>2</sub>P**) structures.

Table 1 Bond lengths and angles of the saddle point structures (**6SP**, **2A6SP**), intermediates **6IP/2A6IP** and equilibrium 6-NO<sub>2</sub> structure in both **6NO<sub>2</sub>P** and **2A6NO<sub>2</sub>P**

	Bond/Å			Angle/°	
	N-O(1)	N-O(2)	O(1)-O(2)	C-N-O(1)	C-N-O(2)
<b>6SP</b>	1.38	1.39	1.74	117.9	116.6
<b>2A6SP</b>	1.44	1.44	1.48	110.1	110.0
<b>6IP</b>	1.44	1.45	1.49	109.8	109.5
<b>2A6IP</b>	1.45	1.44	1.49	109.9	109.8
<b>6NO<sub>2</sub>P</b>	1.23	1.25	2.21	115.9	116.9
<b>2A6NO<sub>2</sub>P</b>	1.23	1.23	2.21	115.9	117.1

structure (**6NO<sub>2</sub>P**) is rotated with respect to the plane of the purine so that the N-C-N-O dihedral angle is 122.9°. This angle is essentially the same for the **2A6NO<sub>2</sub>P** structure.

On the path to the formation of either **6NO<sub>2</sub>P** or **2A6NO<sub>2</sub>P** from the starting complexes **6NP** + O<sub>2</sub> or **2A6NP** + O<sub>2</sub>, respectively, there is a stable intermediate, designated **6IP** or **2A6IP**, shown in Fig. 6. Based on this observation, the oxidation pathway was divided into two NEB calculations, which are shown together in Fig. 7. In the first calculation the starting point has O<sub>2</sub> approximately 4 Å from the nitreno group, **6NP** + O<sub>2</sub> or **2A6NP** + O<sub>2</sub>, and an endpoint at the stable intermediate, **6IP** or **2A6IP**. The second NEB calculation begins from **6IP** or **2A6IP** and ends at **6NO<sub>2</sub>P** or **2A6NO<sub>2</sub>P**. Thus, the molecule must pass through the stable 6-dioxaziridine intermediate structure on the way from the addition of O<sub>2</sub> to the formation of **6NO<sub>2</sub>P** or **2A6NO<sub>2</sub>P**. It is clear from inspection that the final stage of the process involving the rearrangement from **6IP/2A6IP** → **6NO<sub>2</sub>P/2A6NO<sub>2</sub>P** has the same energy change in both the **6NP** and **2A6NP**. Fig. 7 strongly suggests that the **6NO<sub>2</sub>P/2A6NO<sub>2</sub>P** product will be formed if it reaches **6IP/2A6IP**. Since this product is only formed in 2-aminopurine derivative, and the alternative ring-expansion takes place in the purine derivative, we conclude that the differences in reactivity occur in the preceding steps that lead to the formation of the **6IP/2A6IP** intermediates.

In order to investigate the significance of the different peaks and valleys in the energy of the trajectory leading to the formation of the intermediate, three points in the NEB trajectory that were near maxima or minima were chosen for further refinement using the program DIMER, which minimizes the gradient of the structures along the reaction path and thereby locates a saddle point along the trajectory.<sup>15</sup> Once the saddle points were located, the Hessian was calculated for the saddle point geometry. In theory, there should be a single negative eigenvalue corresponding to the point where the minimum energy path from reactants to products reaches the transition

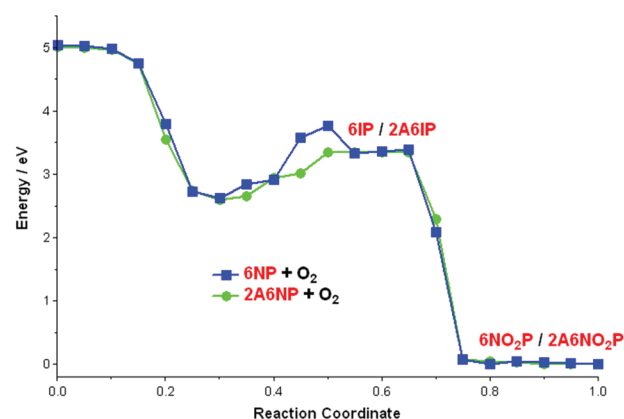
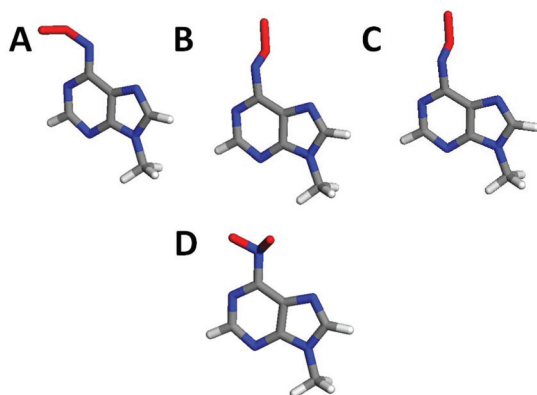


Fig. 7 Energy of the structures in the NEB calculation of the oxidation pathway for 6-nitreno-9-methyl-9H-purine (**6NP**) and 6-nitreno-9-methyl-9H-purin-2-amine (**2A6NP**). The saddle points calculated using DIMER were added to the NEB calculation to obtain a more accurate estimate of the barriers along the reaction path.

state. In practice, there can be additional negative eigenvalues and it is advisable to examine the nature of the saddle point using intrinsic reaction coordinate (IRC) analysis. IRC analysis consists of projections at the transition state along specific normal modes whose Hessian is negative until the gradient along that mode is zero. Such a point should correspond to the reactant or product for reverse and forward projections of the mode, respectively. IRC analysis validates the transition state and identifies the mode that leads from the reactants to the transition state (and on to the products).

In the calculations presented here, the maximum number of negative eigenvalues was three. When more than one negative eigenvalue was found, there was a mode that involved motions that appear to be along a reaction coordinate, but one of the additional negative eigenvalues was found to be a methyl rotation. In the two cases where three negative eigenvalues were found, the third eigenvalue corresponded to a low frequency torsional mode. Using IRC analysis one can validate the saddle points and determine whether the character of the saddle points (transition states) in each molecule is similar or different. Such an analysis provides insights into the nature of saddle points and helps to define which points along the reaction coordinate to true transition states.

Three distinct saddle points were found for both the 6-nitropurine and 6-nitro-9-methyl-9H-purin-2-amine systems when O<sub>2</sub> is allowed to react with these molecules. However, despite their superficial similarities, the intrinsic reaction coordinates and barrier heights for these saddle points were significantly different. The calculated structure for the local energy minimum at the frame of the trajectory for 6NP + O<sub>2</sub> led to a saddle point structure shown in Fig. 8A. This structure consists of an addition of O<sub>2</sub> to the 6-nitro group from the side with an attack perpendicular to the plane of the purine. This structure rearranges to the one shown in Fig. 8B, which consists of a linear O<sub>2</sub> that oscillates from side to side maintaining an orientation parallel to the C-N(6) bond. Finally the



**Fig. 8** Saddle point structures along the reaction pathway for the 6NP + O<sub>2</sub> reaction. The binding energies of these saddle point structures are (A) -88.10 eV, (B) -88.60 eV, (C) -88.6 eV and (D) -87.75 eV, respectively, compared to -91.52 eV for 6-nitro-9-methyl-9H-purine (6NO<sub>2</sub>P). The energies of these structures are (A) 3.42 eV, (B) 2.92 eV, (C) 2.92 eV and (D) 3.77 eV greater than the energy of 6NO<sub>2</sub>P.

bound O<sub>2</sub> rearranges to intermediate 6IP. The structure in Fig. 8D is a saddle point formed after 6IP on the path to 6NO<sub>2</sub>P. There is a barrier that must be surmounted on the path from 6IP to 6NO<sub>2</sub>P, but this further aspect of the reactivity will be considered in a future publication that focuses on a detailed look at the intrinsic reaction coordinate.

The trajectory for O<sub>2</sub> addition in the case of 6-nitro-9-methyl-9H-purin-2-amine consists of a series of 3 saddle points shown in Fig. 9. As was done above for the NEB trajectory of 6NO<sub>2</sub>P, the structures in Fig. 9 were obtained by choosing selected pairs of structures in the NEB calculation shown in Fig. 7 and subjecting them to further refinement using the program DIMER.<sup>13</sup> There is a complex set of rearrangements as the O<sub>2</sub> atom moves into position to form the meta-stable 2A6NO<sub>2</sub>P form. The structures along this pathway for the 2A6NP + O<sub>2</sub> calculation given in Fig. 6 show that the O<sub>2</sub> atom begins the process of addition to nitrene by an attack perpendicular to the purine ring. Subsequently, the O<sub>2</sub> atom rotates to become coplanar with the purine ring. Finally, the O<sub>2</sub> moves to an orientation that is parallel, but shifted out of the purine ring plane. While the structures in Fig. 9B and 9C resemble the structures in Fig. 9A and 9B, respectively, they differ in order and orientation of the O<sub>2</sub> molecule.

The second part of the trajectory involves the rearrangement of the structure 6IP/2A6IP, an intermediate O<sub>2</sub> bonded to the nitrene N atom in a triangular fashion. While there are comparable barriers prior to the formation of this intermediate, the greatest energy barrier is found for the structure in Fig. 8D, which is formed after 6IP in the trajectory. The 6-nitro-9-methyl-9H-purine has a barrier that is 0.42 eV higher than the barrier for 6-nitro-9-methyl-9H-purin-2-amine. No unique saddle point structure was found for a similar calculation following 2A6IP. Instead the saddle point structure converged on the stable intermediate. This difference in barrier following the formation of the stable intermediate is significant since this barrier must slow the formation of the 6-NO<sub>2</sub> group. Consequently, the competing formation of the imidazole-fused 1,3,5-triazepinone nucleoside can take place in 6-nitro-9-methyl-9H-purine, whereas the 6-NO<sub>2</sub> group is formed with high yield in 6-nitro-9-methyl-9H-purin-2-amine. In fact, there are three significant differences between the trajectories in the two cases. There is an energy barrier between

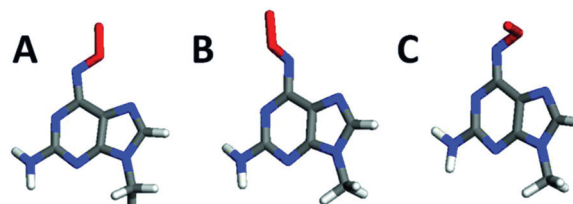


**Fig. 9** Saddle point structures along the reaction pathway for the 2A6NP + O<sub>2</sub> reaction. The binding energies of these saddle point structures are (A) -97.15 eV, (B) -96.86 eV and (C) -96.25 eV, respectively, compared to -99.80 eV for 6-nitro-9-methyl-9H-purin-2-amine (2A6NO<sub>2</sub>P). The energies of these structures are (A) 2.65 eV, (B) 2.94 eV, and (C) 3.55 eV greater than the energy of 2A6NO<sub>2</sub>P.

intermediates A and B in **6NP**, but **2A6NP**. This barrier appears in the NEB calculation as well and is evident in Fig. 7. The second difference is at intermediate C. In **6NP**, intermediate C consists of a double well potential. Although it is quite shallow, it is still significantly deeper than the potential in **8C**.

### The reaction trajectory along the ring expansion pathway

The alternative pathway involves insertion of the nitrene into the purine ring. The starting and ending structures for this pathway are shown in Fig. 10, along with the transition state structure. Fig. 10 shows the purine structures for comparison. It is evident that for the ring expansion to occur in the case of 6-nitreno-9-methyl-9H-purin-2-amine there must be an inversion of the 2-amino group. However, this does not necessarily result in an increased energy barrier for the ring opening process. The energies of these structures and other intermediate structures along this pathway are shown in Fig. 11. The starting energies are 1.08 and 1.33 eV, respectively, for the purine and 2-aminopurine structures. Relative to these initial energies, the barriers to ring expansion are 0.197 and 0.094 eV

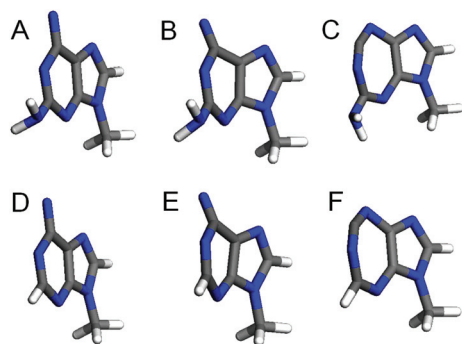


**Fig. 10** Three structures along the ring-opening pathway are shown. The reactant, transition state and product for both 6-nitreno-9-methyl-9H-purin-2-amine (A, B and C respectively) and 6-nitreno-9-methyl-9H-purine (D, E and F, respectively).

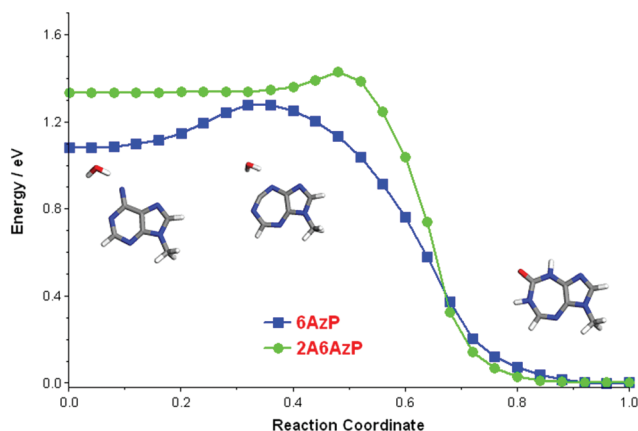


**Fig. 11** Energy of the structures in the NEB calculation of the purine ring expansion pathway for **6AzP** and **2A6AzP**. Three key structures for this pathway, reactant, transition state and product for the **6AzP** are shown. The analogous **2A6AzP** structures are omitted for clarity.

in the case of purine and 2-aminopurine, respectively. In both cases, the transition state structures consist of a bent 6-nitrene that is poised to insert into the ring with a similar geometry. The Mulliken charge and spin density for reactant structures, transition state and ring-expanded product structures are given in Tables S3 and S4 of the ESI.† The major difference between the two species is the spin density on the nitrene, which is significantly greater for 2-aminopurine than for purine.

The energy barrier for ring expansion of **2A6NP** shown in Fig. 11 is smaller than that for **6NP**, which may appear to favor the formation of a ring-expanded form. However, the difference in spin density shown in Tables S3 and S4† creates a spin barrier insertion of the nitrene into an expanded ring for **2A6NP** relative to **6NP**. The required spin change contributes to a smaller electronic factor for 6-nitreno-9-methyl-9H-purin-2-amine than for 6-nitreno-9-methyl-9H-purine, which slows the kinetics of ring expansion. Both the oxidation and ring expansion pathways have lower barriers for 6-nitreno-9-methyl-9H-purin-2-amine. However, it is the competition between the pathways in each molecule that determines the product distribution.

## Conclusions

In conclusion, the above results showed that the near UV light ( $\lambda > 300$  nm) irradiation of 2-amino-6-azidopurine and 6-amino-2-azidopurine ribonucleosides in aqueous solutions in the presence of oxygen led to the efficient formation of their 2- and 6-nitro derivatives. As in the case of aryl azides, the most likely mechanism accounting for the formation of nitropurine ribonucleosides involves a triplet nitrene intermediate that reacts with the  $O_2$  molecule.<sup>16</sup> DFT calculations that compare the reactivity of the **2A6NP** with **6NP** show that the nitrene spin density is significantly higher in the former species. Although the 2-amino group lowers the barrier for oxidation and the barrier for expansion, oxidation is kinetically favored for two reasons. First, the spin density on **6NP** is much larger than in **2A6NP**. Second, there is essentially no barrier for oxidation, while there is still a small barrier for ring expansion in **2A6NP**. The computational results provide a clear interpretation of the experimental results and explain the remarkable difference in reactivity of these two species, which react quantitatively along different pathways.

For the first time, these types of photoproducts were observed *via* UV irradiation of azidonucleosides. The above observations make a significant contribution to understanding the photochemical behavior of the azidopurine ribonucleosides incorporated into oligonucleotides used as photoaffinity labeling probes in the photocross-linking technique.

## Experimental section

### Synthetic and analytical methods

HPLC analysis was performed with an Agilent 1260 Infinity system equipped with diode-array UV-vis detectors. The

column was a ZORBAX SB-C<sub>18</sub>, 5.0 μm, 9.1 × 150 mm, eluted with H<sub>2</sub>O–CH<sub>3</sub>OH using a linear gradient of 16–50% of CH<sub>3</sub>OH over 25 min at a flow rate of 1.8 mL min<sup>-1</sup>. Absorption spectra were measured using a Cary 300 Bio Varian spectrophotometer in CH<sub>3</sub>CN. The HRMS analyses of starting compounds 1–3 and the formed photoproducts were performed using an ESI-TOF system (Bruker). The NMR spectra were measured in CDCl<sub>3</sub> on a Bruker Avance III 700 spectrometer operating at 700 MHz for <sup>1</sup>H and 175 MHz for <sup>13</sup>C. The QCI-P CryoProbe™, 5 mm, was used.

### General procedure for synthesis and spectral data for the substrates

Azidopurine nucleosides 1–3 were synthesized *via* their respective 2- and 6-halogenopurine analogs<sup>17</sup> according to a published procedure.<sup>18</sup> The respective, starting tri-*O*-acetylated halogenopurine nucleoside (1.0 mmol) was dissolved in anhydrous DMF (20 mL) and treated with NaN<sub>3</sub> (4.0 mmol). The reaction mixture was heated at 50 °C for 2 h, cooled, filtrated and concentrated to dryness. The solid residue was dissolved in CH<sub>2</sub>Cl<sub>2</sub> and washed with water. The organic phase was dried over MgSO<sub>4</sub> and evaporated to dryness. The crude product was purified by silica gel column flash chromatography using a gradient of CH<sub>3</sub>OH in CH<sub>2</sub>Cl<sub>2</sub>.

**6-Amino-2-azido-9-(2',3',5'-tri-*O*-acetyl-β-*D*-ribofuranosyl)-purine (1).** Starting nucleoside: 6-amino-2-iodo-9-(2',3',5'-tri-*O*-acetyl-β-*D*-ribofuranosyl)purine. Compound 1 was obtained as white foam (0.75 mmol, 75%). UV (CH<sub>3</sub>CN) λ<sub>max</sub>/nm (ε/M<sup>-1</sup> cm<sup>-1</sup>): 232.0 (25 600), 268.0 (9000), 310.0 (3500) and 322.0 (2700). <sup>1</sup>H NMR: (CDCl<sub>3</sub>) δ 7.88 (s, 1H, H8), 6.13 (d, *J* = 4.9 Hz, 1H, H1'), 5.87 (t, *J* = 5.2 Hz, 1H, H2'), 5.74 (s, 2H, NH<sub>2</sub>), 5.67 (m, 1H, H3'), 4.47 (m, 1H, H5'), 4.45 (m, 1H, H4'), 4.40 (m, 1H, H5''), 2.18–2.11 (s, 9H, CH<sub>3</sub>-Ac). <sup>13</sup>C NMR: (CDCl<sub>3</sub>) δ 170.3–169.4 (C=O-Ac), 157.2 (C6), 156.0 (C2), 151.0 (C4), 138.4 (C8), 117.5 (C5), 86.3 (C1'), 80.0 (C4'), 73.2 (C2'), 70.4 (C3'), 63.1 (C5'), 20.8–20.4 (CH<sub>3</sub>-Ac). HRMS (ESI-TOF): calcd for C<sub>16</sub>H<sub>19</sub>N<sub>8</sub>O<sub>7</sub> [M + H]<sup>+</sup> 435.1377, found 435.1377.

**2-Amino-6-azido-9-(2',3',5'-tri-*O*-acetyl-β-*D*-ribofuranosyl)-purine (2).** Starting nucleoside: 2-amino-6-chloro-9-(2',3',5'-tri-*O*-acetyl-β-*D*-ribofuranosyl)purine. Compound 2 was obtained as white foam (0.7 mmol, 70%). UV (CH<sub>3</sub>CN) λ<sub>max</sub>/nm (ε/M<sup>-1</sup> cm<sup>-1</sup>): 238.0 (6200), 271.0 (7800) and 299.0 (8500). <sup>1</sup>H NMR: (CDCl<sub>3</sub>) δ tetrazole form: 8.02 (s, 1H, H8), 6.62 (s, 2H, NH<sub>2</sub>), 6.01 (m, 1H, H1'), 5.97 (m, 1H, H2'), 5.78 (m, 1H, H3'), 4.45 (m, 1H, H5'), 4.43 (m, 1H, H4'), 4.38 (m, 1H, H5''), 2.17–2.10 (s, 9H, CH<sub>3</sub>-Ac); azido form: 7.99 (s, 1H, H8), 6.13 (m, 1H, H1'), 6.00 (m, 1H, H2'), 5.74 (m, 1H, H3'), 5.13 (s, 2H, NH<sub>2</sub>), 4.53 (m, 1H, H5'), 4.49 (m, 1H, H4'), 4.47 (m, 1H, H5''), 2.17–2.10 (s, 9H, CH<sub>3</sub>-Ac). <sup>13</sup>C NMR: (CDCl<sub>3</sub>) δ tetrazole form: 170.8–170.6 (C=O-Ac), 159.3 (C6), 153.7 (C2), 143.2 (C4), 139.6 (C8), 118.8 (C5), 86.5 (C1'), 79.8 (C4'), 72.7 (C2'), 70.5 (C3'), 62.9 (C5'), 20.8–20.4 (CH<sub>3</sub>-Ac); azido form: 169.7–169.4 (C=O-Ac), 162.6 (C6), 146.1 (C2), 142.6 (C4), 138.9 (C8), 114.9 (C5), 87.2 (C1'), 80.1 (C4'), 72.9 (C2'), 70.6 (C3'), 63.1 (C5'), 20.8–20.4 (CH<sub>3</sub>-Ac). HRMS (ESI-TOF): calcd for C<sub>16</sub>H<sub>19</sub>N<sub>8</sub>O<sub>7</sub> [M + H]<sup>+</sup> 435.1377, found 435.1374.

**2,6-Diazido-9-(2',3',5'-tri-*O*-acetyl-β-*D*-ribofuranosyl)purine (3).** Starting nucleoside: 6-chloro-2-iodo-9-(2',3',5'-tri-*O*-acetyl-β-*D*-ribofuranosyl)purine. Compound 3 was obtained as yellow foam (0.61 mmol, 61%). UV (CH<sub>3</sub>CN) λ<sub>max</sub>/nm (ε/M<sup>-1</sup> cm<sup>-1</sup>): 244.0 (21 000), 266.0 (8700) and 296.0 (11 200). <sup>1</sup>H NMR: (CDCl<sub>3</sub>) δ 8.06 (s, 1H, H8), 6.15 (d, *J* = 5.1 Hz, 1H, H1'), 5.83 (t, *J* = 5.5 Hz, 1H, H2'), 5.60 (t, *J* = 5.3 Hz, 1H, H3'), 4.47 (m, 1H, H4'), 4.42 (m, 2H, H5', H5''), 2.17–2.08 (s, 9H, Ac). <sup>13</sup>C NMR: (CDCl<sub>3</sub>) δ 170.2–169.2 (C=O, Ac), 156.4 (C2), 154.1 (C6), 153.3 (C4), 141.5 (C8), 121.7 (C5), 86.2 (C1'), 80.2 (C4'), 73.0 (C3'), 70.3 (C2'), 62.8 (C5'), 20.7–20.3 (CH<sub>3</sub>-Ac). HRMS (ESI-TOF): calcd for C<sub>16</sub>H<sub>17</sub>N<sub>10</sub>O<sub>7</sub> [M + H]<sup>+</sup> 461.1276, found 461.1280.

### General procedure for UV irradiation

Solutions of compounds 1–3 in an H<sub>2</sub>O–CH<sub>3</sub>CN mixture (9/1, v/v) were photoirradiated at λ > 300 nm under aerobic and anaerobic (Ar atmosphere) conditions in a 0.2 cm UV cell using a 200 W, high-pressure Hg lamp (HBO 200) equipped with a 313 nm interference filter, at room temperature. The progress of the photoreaction was monitored by the disappearance of the absorption band in the UV spectra of compounds 1–3 and by HPLC. To isolate and fully characterize the photoproducts by spectral methods, solutions of compounds 1–3 (5.0 × 10<sup>-4</sup> mol dm<sup>-3</sup>) were irradiated in a 200 mL photoreactor with a 200 W, high-pressure immersion Hg lamp (HBO 200) equipped with a cut-off Pyrex filter (λ > 300 nm). The photoproducts formed were isolated and purified by preparative reversed-phase HPLC.

### Spectral data for the photoproducts

**2,6-Diamino-9-(2',3',5'-tri-*O*-acetyl-β-*D*-ribofuranosyl)purine (4).** UV (CH<sub>3</sub>CN) λ<sub>max</sub>/nm (ε/M<sup>-1</sup> cm<sup>-1</sup>): 216.0 (16 300), 258.0 (8600) and 280.0 (8800). <sup>1</sup>H NMR: (CDCl<sub>3</sub>) δ 7.64 (s, 1H, H8), 5.99 (m, 1H, H1'), 5.97 (t, *J* = 4.7 Hz, 1H, H2'), 5.81 (t, *J* = 5.2 Hz, 1H, H3'), 5.69 (s, 2H, NH<sub>2</sub>-2), 4.92 (s, 2H, NH<sub>2</sub>-6), 4.46 (m, 1H, H5'), 4.42 (m, 1H, H4'), 4.37 (m, 1H, H5''), 2.14–2.09 (s, 9H, CH<sub>3</sub>-Ac). <sup>13</sup>C NMR: (CDCl<sub>3</sub>) δ 170.6–169.5 (C=O-Ac), 159.9 (C6), 155.9 (C2), 151.6 (C4), 136.4 (C8), 114.6 (C5), 86.2 (C1'), 79.8 (C4'), 72.9 (C2'), 70.6 (C3'), 63.1 (C5'), 20.8–20.5 (CH<sub>3</sub>-Ac). HRMS (ESI-TOF): calcd for C<sub>16</sub>H<sub>21</sub>N<sub>6</sub>O<sub>7</sub> [M + H]<sup>+</sup> 409.1472, found 409.1471.

**6-Amino-2-nitro-9-(2',3',5'-tri-*O*-acetyl-β-*D*-ribofuranosyl)-purine (5).** UV (CH<sub>3</sub>CN) λ<sub>max</sub>/nm (ε/M<sup>-1</sup> cm<sup>-1</sup>): 236.0 (12 400), 262.0 (8000) and 332.0 (2700). <sup>1</sup>H NMR: (CDCl<sub>3</sub>) δ 8.19 (s, 1H, H8), 6.26 (d, *J* = 5.5 Hz, 1H, H1'), 6.18 (s, 2H, NH<sub>2</sub>), 5.79 (t, *J* = 5.5 Hz, 1H, H2'), 5.67 (m, 1H, H3'), 4.54 (m, 1H, H4'), 4.50 (m, 1H, H5'), 4.48 (m, 1H, H5''), 2.21–2.12 (s, 9H, CH<sub>3</sub>-Ac). <sup>13</sup>C NMR: (CDCl<sub>3</sub>) δ 170.3–169.6 (C=O-Ac), 155.9 (C6), 155.4 (C2), 149.8 (C4), 141.8 (C8), 122.1 (C5), 86.6 (C1'), 80.9 (C4'), 73.7 (C2'), 70.8 (C3'), 63.2 (C5'), 20.8–20.4 (CH<sub>3</sub>-Ac). HRMS (ESI-TOF): calcd for C<sub>16</sub>H<sub>19</sub>N<sub>6</sub>O<sub>9</sub> [M + H]<sup>+</sup> 439.1214, found 439.1215.

**2-Amino-6-nitro-9-(2',3',5'-tri-*O*-acetyl-β-*D*-ribofuranosyl)-purine (7).** UV (CH<sub>3</sub>CN) λ<sub>max</sub>/nm (ε/M<sup>-1</sup> cm<sup>-1</sup>): 230.0 (14 900) and 386.0 (2900). <sup>1</sup>H NMR: (CDCl<sub>3</sub>) δ 8.17 (s, 1H, H8), 6.11 (d, *J* = 4.9 Hz, 1H, H1'), 5.97 (t, *J* = 5.2 Hz, 1H, H2'), 5.74

(t,  $J = 4.9$  Hz, 1H, H3'), 5.62 (s, 2H, NH<sub>2</sub>), 4.49 (m, 1H, H4'), 4.47 (m, 1H, H5'), 4.42 (m, 1H, H5''), 2.16–2.10 (s, 9H, CH<sub>3</sub>-Ac). <sup>13</sup>C NMR: (CDCl<sub>3</sub>)  $\delta$  170.5–169.3 (C=O-Ac), 158.6 (C6), 158.3 (C2), 152.4 (C4), 144.8 (C8), 119.5 (C5), 86.8 (C1'), 80.2 (C4'), 72.7 (C2'), 70.4 (C3'), 62.8 (C5'), 20.7–20.4 (CH<sub>3</sub>-Ac). HRMS (ESI-TOF): calcd for C<sub>16</sub>H<sub>19</sub>N<sub>6</sub>O<sub>9</sub> [M + H]<sup>+</sup> 439.1214, found 439.1239.

### Computational methods

Solutions DFT calculations were carried out using the DMol3 code, which implements a numerical basis set. The geometry optimizations, the NEB method and thermodynamic free energies were calculated using DMol3<sup>13</sup> with the PBE functional<sup>19</sup> and the DNP basis set.

The NEB method<sup>20</sup> was employed using a linear interpolation of structures as the starting point. A linear interpolation was achieved using the Reaction Preview tool in Materials Studio, which ensures a one-to-one correspondence of the atoms in the initial and final structures. The initial and final structures were geometry optimized using the same basis set and functional as those used for the NEB calculation with a convergence criterion of  $<10^{-6}$  change in the energy (in Hartrees) between two optimization steps. The NEB chains used in the calculation consisted of 16–30 structures. The end point structures were held fixed and the intervening structures were iteratively subjected to the NEB method until the convergence criterion of a less than  $5 \times 10^{-4}$  Hartrees Bohr<sup>-1</sup> change in the gradient was reached. Refinement of saddle points was calculated using a version of the program DIMER.<sup>15a</sup> The FIRE optimizer was employed in the iterative calculations.<sup>21</sup>

Three paths were defined using the Reaction Preview tool. The starting structures consisted of geometry optimized purines with an O<sub>2</sub> molecule poised approximately 4 Å from the 6-nitrene of the purine ring system. The end point for the first stage consists of a geometry optimized intermediate (**6IP** or **2A6IP**). A second path begins at **6IP/2A6IP** and ends at **6NO<sub>2</sub>P/2A6NO<sub>2</sub>P**. These paths were compared to the ring expansion path that involves insertion of the 6-nitrene into the ring. Structures along these paths that appear to be local maxima were selected in pairs and submitted to the program DIMER for further optimization of the structures to locate saddle points. In order to test whether saddle points have been located, the structures refined in DIMER were submitted for a vibrational frequency calculation. Ideally the saddle point has one negative eigenvalue. In cases where more than one negative eigenvalue was observed, the potential surfaces and projections along relevant eigenvectors were studied. Finally, intrinsic reaction coordinate (IRC) analysis was conducted to ascertain that the transition state was correctly identified and to determine which eigenvector follows the minimum energy path.

### Abbreviations

6AzP 6-Azido-9-methyl-9H-purine  
2A6AzP 6-Azido-9-methyl-9H-purin-2-amine

TP 7-Methyl-7H-tetrazolo[5,1-*f*]purine  
2ATP 7-Methyl-7H-tetrazolo[5,1-*f*]purin-5-amine  
6NP 6-Nitreno-9-methyl-9H-purine  
2A6NP 6-Nitreno-9-methyl-9H-purin-2-amine  
6IP 6-Dioxaziridino-9-methyl-9H-purine  
2A6IP 6-Dioxaziridino-9-methyl-9H-purin-2-amine  
6SP 6-Dioxaziridino-9-methyl-9H-purine transition state  
2A6SP 6-Dioxaziridino-9-methyl-9H-purin-2-amine transition state  
6NO<sub>2</sub>P 6-Nitro-9-methyl-9H-purine  
2A6NO<sub>2</sub>P 6-Nitro-9-methyl-9H-purin-2-amine

### Notes and references

- (a) M. M. Hanna, *Methods Enzymol.*, 1989, **180**, 383; (b) L. A. Sylvers and J. Wower, *Bioconjugate Chem.*, 1993, **4**, 411; (c) J. Wower, K. V. Rosen, S. S. Hixon, R. A. Zimmermann, L. A. Sylvers and Y. Xing, *Bioconjugate Chem.*, 1994, **5**, 158; (d) M. M. Hanna, L. Bensten, M. Lucido and A. Sapre, *Methods Mol. Biol.*, 1999, **118**, 21.
- K. M. Meisenheimer and T. H. Koch, *Crit. Rev. Mol. Biol.*, 1997, **32**, 101.
- (a) S. Senda, K. Hirota, M. Suzuki, T. Asao and K. Maruhashi, *J. Chem. Soc., Chem. Commun.*, 1976, 731; (b) S. Senda, K. Hirota, T. Asao and K. Maruhashi, *J. Am. Chem. Soc.*, 1977, **99**, 7358; (c) S. Senda, K. Hirota, T. Asao and K. Maruhashi, *J. Chem. Soc., Chem. Commun.*, 1978, 367; (d) S. Senda, K. Hirota, T. Asao and K. Maruhashi, *J. Am. Chem. Soc.*, 1978, **100**, 7661; (e) S. Senda, K. Hirota, T. Asao and K. Maruhashi, *J. Chem. Soc., Perkin Trans. 1*, 1984, 1719; (f) H. Tanaka, H. Hayakawa, K. Haraguchi and T. Miyasaka, *Nucleosides Nucleotides*, 1985, **4**, 607; (g) T. Miyasaka, H. Tanaka, K. Satoh, M. Imahashi, K. Yamaguchi and Y. Iitaka, *J. Heterocycl. Chem.*, 1987, **24**, 873; (h) F. Peyrane, M. Cesario and P. Clivio, *J. Org. Chem.*, 2006, **71**, 1742; (i) S. Goudain, A. Martinez, C. Petermann, D. Harakat and P. Clivio, *J. Org. Chem.*, 2009, **74**, 6885; (j) S. Goudain, C. Petermann, A. Martinez, D. Harakat and P. Clivio, *J. Org. Chem.*, 2011, **76**, 1906.
- Y. Xing, S. S. Hixson and R. A. Zimmermann, *Tetrahedron Lett.*, 1990, **31**, 5849.
- S. N. Bose, *Indian J. Chem.*, 1984, **23B**, 677.
- K. Komodziński, J. Nowak, J. Lepczyńska, J. Milecki and B. Skalski, *Tetrahedron Lett.*, 2012, **53**, 2316.
- K. Komodziński, J. Lepczyńska, P. Ruszkowski, J. Milecki and B. Skalski, *Tetrahedron Lett.*, 2013, **54**, 3781.
- J. A. Montgomery and L. B. Holum, *J. Am. Chem. Soc.*, 1958, **80**, 404.
- T. Kaiya, H. Tanaka and K. Kohda, *Nucleosides, Nucleotides Nucleic Acids*, 2002, **21**, 427.
- (a) C. Temple, M. C. Thorpe, W. C. Colburn and J. A. Montgomery, *J. Org. Chem.*, 1966, **31**, 935; (b) C. Mathe, T. Lioux and G. Gosselin, *Nucleosides, Nucleotides Nucleic Acids*, 2003, **22**, 605; (c) T. Lioux, G. Gosselin and C. Mathe, *Eur. J. Org. Chem.*, 2003, 3997.

- 11 (a) C. Temple, L. C. Kussner and J. A. Montgomery, *J. Org. Chem.*, 1966, **31**, 2210; (b) A. Masternak, B. Skalski and J. Milecki, *J. Labelled Compd. Radiopharm.*, 2007, **50**, 43; (c) M. K. Lakshman, M. K. Singh, D. Parrish, R. Balachandran and B. W. Day, *J. Org. Chem.*, 2010, **75**, 2461.
- 12 T. Fujii and T. Itaya, *Heterocycles*, 1999, **51**, 1971.
- 13 (a) B. Delley, *J. Chem. Phys.*, 1990, **92**, 508; (b) B. Delley, *J. Chem. Phys.*, 2000, **113**, 7756.
- 14 (a) R. A. McClelland, P. A. Davidse and G. Hadzialic, *J. Am. Chem. Soc.*, 1995, **117**, 4173; (b) B. Cheng and R. A. McClelland, *Can. J. Chem.*, 2001, **79**, 1881; (c) V. Voskresenska, R. M. Wilson, M. Panov, A. N. Tarnovsky, J. A. Krause, S. Vyas, A. H. Winter and C. M. Hadad, *J. Am. Chem. Soc.*, 2009, **131**, 11535.
- 15 (a) G. Henkenlman and H. Jonsson, *J. Chem. Phys.*, 1999, **111**, 7010; (b) R. A. Olsen, G. J. Kroes, G. Henkelman, A. Arnaldsson and H. Jonsson, *J. Chem. Phys.*, 2004, **121**, 9776.
- 16 (a) B. Singh and J. S. Brinen, *J. Am. Chem. Soc.*, 1971, **93**, 540; (b) J. S. Brinen and B. Singh, *J. Am. Chem. Soc.*, 1971, **93**, 6623; (c) R. A. Abramovitch and S. R. Challand, *J. Chem. Soc., Chem. Commun.*, 1972, 964; (d) T. Hander, P. Wessig, J. Bendig and R. Stosser, *J. Am. Chem. Soc.*, 1999, **121**, 6580; (e) J. Liu, C. M. Hadad and M. S. Platz, *Org. Lett.*, 2005, **7**, 549.
- 17 (a) M. J. Moris and B. Uznański, *Can. J. Chem.*, 1981, **59**, 2601; (b) V. Nair and S. G. Richardson, *Synthesis*, 1982, 670; (c) A. Matsuda, M. Shizozaki, M. Suzuki, K. Watanabe and T. Miyasaka, *Synthesis*, 1986, 385.
- 18 L. P. Kotra, K. K. Manouilov, E. Cretton-Scott, J.-P. Sommadossi, F. D. Boudinot, R. F. Schinazi and C. K. Chu, *J. Med. Chem.*, 1996, **39**, 5202.
- 19 J. P. Perdew, K. Burke and M. Ernzerhof, *Phys. Rev. Lett.*, 1996, **77**, 3865.
- 20 D. Sheppard, R. Terrell and G. Henkelman, *J. Chem. Phys.*, 2008, **128**, 134106.
- 21 E. Bitzek, P. Koskinen, F. Gahler, M. Moseler and P. Gumbsch, *Phys. Rev. Lett.*, 2006, **97**, 170201.